Macromolecules
ARTICLE

Macromolecules **2009**, *42*, 8435–8442 **8435**
DOI: 10.1021/ma901523w

Concentration Fluctuations, Local Order, and the Collective Structure of Polymer Nanocomposites

Lisa M. Hall,[†] Benjamin J. Anderson,[†,§] Charles F. Zukoski,[†,‡] and Kenneth S. Schweizer*[,†,‡]

[†]*Department of Chemical & Biomolecular Engineering and* [‡]*Department of Materials Science, University of Illinois, 1304 W. Green Street, Urbana, Illinois 61801.* [§] *Present address: Sandia National Laboratories, Albuquerque, NM 87185-1245.*

Received July 13, 2009; Revised Manuscript Received August 19, 2009

ABSTRACT: A combined theory−experiment analysis of adsorbing polymer mediated structural reorganization of silica nanoparticles in equilibrated and miscible poly(ethylene oxide) (PEO) and polytetrahydrofuran (PTHF) nanocomposites is presented. Quantitative comparison of microscopic liquid state theory calculations with small-angle X-ray scattering experiments demonstrate the theoretical approach properly accounts for the effects of adsorbed polymer layers on nanoparticle concentration fluctuations over all length scales for a wide range of volume fractions and interfacial cohesion strengths. The mixture total packing fraction is increased as particles are added to the polymer melt in order to account for equation-of-state effects which are important at very high filler loadings. A distinctive microphase separation like peak in the collective polymer structure factor is predicted. Nanoparticle potential of mean force calculations suggest a criterion for the onset of depletion or bridging induced kinetic gelation which is consistent with the observation of complete miscibility for the PEO system but nonequilibrium behavior in the PTHF nanocomposite.

I. Introduction

Polymer nanocomposites (PNC) are an emerging class of hybrid materials composed of hard nanoparticles or "fillers" dispersed in a soft polymer matrix.[1] Their high surface-to-volume ratio allows nanoparticles at relatively low volume fractions to strongly modify the polymer matrix, resulting in improved mechanical, optical, thermal, and other bulk properties. Of critical importance is to control the polymer−filler interface, and good nanoparticle spatial dispersion is often desired.[1,2] A deep understanding of the relationship between the physical and chemical attributes of individual particles and polymers, collective mixture structure, and phase behavior is needed to fully realize the engineering potential of these materials.

From a fundamental physics perspective, a dense amorphous mixture composed of many high radius of curvature hard particles in contact with adsorbing random coil chains is a fascinating statistical mechanics problem. Recently, the first principles polymer reference interaction site model (PRISM) theory[3] has been generalized[4,5] to PNCs, thereby providing a microscopic description of pair correlations, scattering functions, thermodynamics, and phase behavior. A very rich behavior is predicted for the minimalist model of hard spheres in a homopolymer melt. The strength (ε_{pn}) and spatial range of the monomer−particle attraction play a critical role in determining whether polymers mediate depletion aggregation (entropy-driven, high-temperature phase separation), steric stabilization and good dispersion (homogeneous liquid), or local bridging of nanoparticles (enthalpy-driven, low-temperature demixing). The most striking prediction is that for intermediate ε_{pn} values thermodynamically stable "bound polymer layers" form around nanoparticles, resulting in a repulsive potential of mean force and a "miscibility window" in the phase diagram.[5] This result has recently been *qualitatively* confirmed for equilibrated silica−poly(ethylene oxide) (PEO) nanocomposites under index matching conditions which satisfy the hard filler criterion.[6,7] The identification of this experimental system affords the opportunity to use small-angle X-ray scattering (SAXS) to probe the theoretical structure predictions for model hard-sphere fillers over a wide range of length scales and volume fractions. Scattering of silica nanoparticles in the more hydrophobic, less strongly adsorbing polytetrahydrofuran (PTHF) matrix is also measured and compared to PRISM theory calculations.

The primary focus of the present study is to *quantitatively* confront theory and experiment for the silica−PEO and silica−PTHF nanocomposites and establish how polymers mediate many-body correlations between nanoparticles in the presence of variable interfacial cohesion. To achieve this goal, a new theoretical model is developed that adjusts the total mixture packing fraction as fillers are added to the homopolymer matrix in order to mimic equation-of-state effects expected to be operative at constant pressure. Special attention is paid to the packing fraction dependence of the particle osmotic compressibility (amplitude of long wavelength concentration fluctuations) and the intensity and location of the wide-angle peak in the nanoparticle structure factor that quantifies the degree of local cage order and its characteristic length scale. We demonstrate that the theoretical results for these quantities compare quite well to experimental observations. Moreover, for the short unentangled chains studied, both theory and experiment show little dependence on molecular weight and exhibit a strong dependence on the chemically specific interfacial attraction strength.

The remainder of the paper is structured as follows. The experimental materials and measurements are briefly discussed in section II. Section III summarizes the nanocomposite model and statistical mechanical theory, and the new adjusted packing fraction approach is formulated and representative model calculations based on it are presented. Theory and experiment for the filler collective scattering patterns are quantitatively compared in section IV, and predictions are made for the polymer collective

*Corresponding author. E-mail: kschweiz@illinois.edu.

Published on Web 08/27/2009

scattering function for the same experimental systems in section V. Calculations of the real space polymer-mediated potential of mean force between silica fillers in PEO and PTHF are given in section VI and employed to qualitatively explore possible kinetic arrest phenomena. The paper concludes with a summary in section VII.

II. Experimental System and Measurements

Details of the experimental sample preparation and SAXS measurements of the collective nanoparticle (silica) structure factor, $S_{nn}(k)$, are documented elsewhere.[6,7] The three polymers studied are PEO of molecular weights (MW) 400 and 1000, and polytetrahydrofuran (PTHF) of MW = 1000, all obtained from Sigma-Aldrich. These low molecular weight polymers are all below the entanglement threshold of the pure polymer melts, thereby allowing the equilibration essential for comparison with the equilibrium theory. The silica particles were produced using the Stöber process and had a volume averaged diameter of $D = 44 \pm 4$ nm. The polymers are well contrast matched with the nanoparticles, leading to minimal van der Waals attractions between fillers. Scattering experiments were performed at 75 °C.

To create a composite sample, the silica particles were first synthesized in ethanol solution and concentrated to a desired mass fraction. This solution was then mixed with polymer, and the solvent evaporated under conditions chosen to best disperse the particles. Filler volume fraction was computed using the measured composite density, silica density, and particle and polymer masses. The filler structure factor was determined by subtracting the pure polymer scattering intensity from the total composite SAXS intensity, assuming that cross-terms can be neglected since the particle X-ray scattering is dominant. The collective nanoparticle structure factor was then determined in the standard manner by dividing the concentrated particle scattering intensity by its volume fraction weighted dilute particle limit analogue.

The characteristic ratio for a chain of n backbone bonds, C_n, has been measured for PEO at large MW (110K) using neutron scattering and found to be 5.7 at 74 °C; the structurally similar PTHF should have a similar C_n.[8] Theoretical calculations for PEO yield a characteristic ratio of ~5.4 in the long chain limit, which decreases to ~5.0 (4.5) for PEO composed of 68 (27) backbone bonds.[9] The backbone chemical bond length is approximately $l_b \approx 0.15$ nm, and the angle between adjacent bonds is 68°.[10] The number of backbone bonds is ~27 for PEO 400, ~68 for PEO 1000, and ~70 for PTHF 1000. These values motivate the choice of chain length in the theoretical calculations.

III. Theory and Model

A. Background. The mixture model and theory employed are identical to prior studies.[4,5] PRISM theory for a homopolymer nanocomposite consists of three coupled nonlinear integral equations[4,5] for the site−site intermolecular pair correlation functions, $g_{ij}(r)$, where i and j refer to polymer monomer (p) or nanoparticle (n).[3,4] The nanoparticles are spheres of diameter D, and the polymer is modeled as a freely jointed chain (FJC) composed of N identical spherical interaction sites. The Fourier transform of the intramolecular probability distribution function, or structure factor, is given by[3]

$$\omega_p(k) = [1 - f^2 - 2N^{-1}f + 2N^{-1}f^{N+1}]/(1-f)^2 \quad (1)$$

where $f = \sin(kl_p)/(kl_p)$, and the persistence (bond) length $l_p = {}^4/_3 d$ (typical of flexible polymers).[3,11] The generalized Ornstein−Zernike or Chandler−Andersen matrix equations relate the site−site intermolecular pair correlation function, g, to the site−site intermolecular direct correlation function, C, as[3,12]

$$\mathbf{H}(k) = \Omega(k)\mathbf{C}(k)[\Omega(k)+\mathbf{H}(k)] \quad (2)$$

The diagonal matrix $\mathbf{\Omega}(k)$ contains the elements $\rho_t\omega_t(k)\delta_{ij}$, $\mathbf{C}(k)$ consists of the elements $C_{ij}(k)$, and $\mathbf{H}(k)$ is composed of the elements $\rho_i\rho_j h_{ij}(k)$, where $h_{ij}(r) = g_{ij}(r) - 1$. The number densities are $\rho_p = \eta_p/(d^3\pi/6)$ and $\rho_n = \eta_n/(D^3\pi/6)$, where η_p and η_n are the polymer and particle packing fractions, respectively, determined as discussed in the next section.

The site−site Percus−Yevick closure approximation (eq 3) is used for polymer−polymer (p−p) and polymer−nanoparticle (p−n) correlation functions, while the hypernetted chain (HNC) closure (eq 4) is used for the nanoparticle−nanoparticle correlation functions.

$$C_{ij}(r) = (e^{-U_{ij}(r)} - 1)(1 + h_{ij}(r) - C_{ij}(r)) \quad (3)$$

$$C_{nn}(r) = e^{h_{nn}(r) - C_{nn}(r) - U_{nn}(r)} - 1 - h_{nn}(r) + C_{nn}(r) \quad (4)$$

This choice of closures yields good agreement with simulations in the dilute one- and two-particle limits.[13] In eqs 3 and 4, U_{ij} are the pair decomposable site−site potentials, where U_{nn} and U_{pn} are taken to be *purely* hard core. The chemical nature of the PNC enters via the two parameters of an attractive interfacial potential: the strength at contact ε_{pn} (in units of thermal energy) and spatial range α (in units of the monomer diameter). Beyond the hard core distance of closest approach, the exponential interfacial potential is given by

$$U_{pn}(r) = -\varepsilon_{pn} \exp\left(\frac{-(r-(D+d)/2)}{\alpha d}\right) \quad (5)$$

Within the present model, ε_{pn} qualitatively determines the free energy change associated with transferring a monomer from the pure monomer fluid environment to the surface of a nanoparticle. In the language of traditional polymer mean field theory, this energy parameter sets the scale of a monomer level *bare* energetic "chi-parameter". Henceforth, all lengths (energies) are expressed in units of the monomer diameter (thermal energy).

An inexact Newton's method is employed to numerically solve the coupled nonlinear PRISM integral equations[5] which yield the real space pair correlation functions, $g_{ij}(r)$. The polymer and nanoparticle collective partial structure factors are given by

$$\mathbf{S}'(k) = \Omega(k) + \mathbf{H}(k) = (\mathbf{I} - \Omega(k)\mathbf{C}(k))^{-1}\Omega(k) \quad (6)$$

where $\mathbf{I}$ is the identity matrix and $\mathbf{S}'$ is the dimensionalized version of $\mathbf{S}$, given by $S'_{ii} = \rho_i S_{ii}$. Macroscopic liquid−liquid spinodal phase separation is signaled by the divergence of all partial structure factors at $k = 0$. In practice, the spinodal phase boundary is numerically inferred from the small wavevector upturn in the structure factor at values of ε_{pn} just before the equations cease to numerically converge. The spinodal phase boundary reported here is the last ε_{pn} which could be converged based on increments of 0.0001 as discussed previously;[5] the difference between this value and an estimate of the spinodal location obtained by extrapolating $1/S_{nn}(k=0)$ or $1/S_{pp}(k=0)$ to zero (as often done experimentally) is not generally visible on the scale of the plots presented.

The degree of polymerization is $N = 10$ or 100, the size asymmetry ratio $D/d = 10$, and the spatial range of attraction is $\alpha = 0.5$. These are typical values as motivated in prior work[4,5] and as such were *not* fine-tuned for comparison to the present experimental data. Note that $N = 10$ is roughly the number of monomers for PEO 400. The strength of the interfacial cohesion is varied widely ($0 \le \varepsilon_{pn} \le 4$) in order to construct the spinodal phase diagram, and detailed analysis

is performed for selected values that are relevant to the nanoparticle structure factors measured experimentally.

To further motivate the chosen values of N, consider the mapping of a polymer chain onto the FJC model. A standard approach is to require that the FJC model reproduces the largest length scales of the real polymer: the end-to-end distance and contour length. This mapping yields a statistical segment length of $C_n l_b \sim 0.75$ nm for PEO. The corresponding number of segments $N = N_{bb}/C_n$, where N_{bb} is the number of backbone bonds. For PEO 400 and 1000, $N_{bb} = 27$ and 68, while $C_n \sim 5$, which implies $N \sim 5$ and 13. However, a mapping based on global chain properties is not the most relevant for dense polymer melts or mixtures where packing effects are controlled by the local chain stiffness. The latter is characterized by the persistence length, $l_p = (C_n + 1)l_b/2 \sim 3l_b$, or one PEO monomer. This mapping then implies $N \sim 10$ and 25 for the two PEO samples, and the FJC "site" corresponds to one monomer yielding roughly $d \sim 0.6$ nm.

Modest changes in persistence length, α, and D/d were briefly investigated but did not significantly modify the theoretical results, although increasing D/d makes the PRISM equations numerically more difficult to converge. We report calculations only for $\alpha = 0.5$ and $D/d = 10$ in order to realize our goal of employing just one material-specific adjustable parameter to perform the quantitative theory−experiment confrontation, while at the same time allowing comparison with prior published PRISM results.[5] Calculations for both $N = 10$ and 100 are presented, focusing on $N = 100$ as in prior studies; these two values of N essentially bracket the relevant values for the two PEO samples studied experimentally, and the sensitivity on N is weak.

B. Adjusted Packing Fraction Description. The final input to the theory is the monomer and particle packing fractions: $\eta_p \equiv \pi\rho_p d^3/6$ and $\eta_n \equiv \pi\rho_n D^3/6$. For simplicity, and due to the lack of a constant pressure mixture equation-of-state, theoretical studies have previously assumed a fixed melt-like *total* packing fraction of $\eta_t \equiv \eta_p + \eta_n = 0.4$[4,5] or 0.5.[14,15] However, recent experiments[6] have been performed well beyond these values, up to *filler* packing fractions of ~0.55. Physically, we expect the interstices between nanoparticle surfaces are densely filled by monomers in real materials held at constant (atmospheric) pressure. This implies η_t should increase with nanoparticle volume fraction, in analogy with mixtures of small and large hard spheres.[16] We propose to account for this packing effect in a minimalist, but physically motivated and *no adjustable parameter*, manner. Specifically, for the pure polymer melt $\eta_{p0} = 0.4$ is employed since it yields a realistic dimensionless isothermal compressibility, $S_{pp}(k=0) \sim 0.2$, based on PRISM theory for a hard core FJC fluid.[3,4] The polymer packing fraction *outside* the volume excluded by nanoparticles is assumed to remain the same as in the pure melt, thereby yielding an "adjusted" total packing fraction of

$$\eta_t = \eta_n + \eta_{p0}(1 - \eta_n(1+(d/D))^3) \quad (7)$$

This equation neglects the consequences of overlap of the excluded volume shells of nearby particles. A more accurate expression for the free volume, which has been employed in the study of hard sphere mixtures, yields a similar η_t at the large D/d and reasonable η_n values studied here.[16,17] The packing fraction of atomic hard-sphere mixtures can also in principle be predicted by density functional theory[18] or the PY equation of state at constant pressure.[19] However, there are virtually no simulation or experimental data for polymer nanocomposite densities as a function of mixture composition that would allow quantitative comparison with our model, which makes it difficult to justify the use of more complicated adjustments of η_t as a function of η_n in this initial study. Moreover, the accurate computation of an equation of state using integral equation theory is generically difficult and is particularly not appropriate for our model based on a single *effective* polymer−particle attraction.

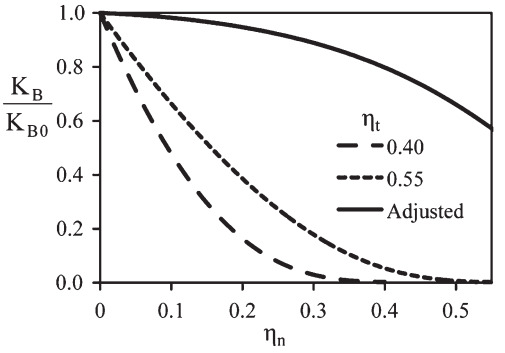

Figure 1. Theoretical bulk modulus normalized by its pure polymer melt value as a function of filler packing fraction for the three indicated mixture total packing fraction models. System parameters are $N = 100$, $D/d = 10$, $\alpha = 0.5$, and $\varepsilon_{pn} = 0.5$.

As a first test of the adjusted packing fraction concept and demonstration of its importance at high filler volume fractions, we compute the mixture bulk modulus, K_B. This property follows from the direct correlation functions as $k \to 0$.[4]

$$\frac{K_B}{kT} = \frac{\rho_p}{N} + \rho_n - \rho_p{}^2 C_{pp}(0) - \rho_n{}^2 C_{nn}(0) - 2\rho_p\rho_n C_{pn}(0) \quad (8)$$

In the pure polymer melt limit, the dimensionless (units of kT/d^3) $K_B = 4.49$ for $\eta_t = 0.4$ and $K_B(\eta_n = 0) = 29.9$ for $\eta_t = 0.55$. Using $d \sim 0.6$ nm yields reasonable dimensional values of the bulk modulus of the pure polymer.

Calculations of the nanocomposite bulk modulus divided by its pure polymer melt value as a function of nanoparticle volume fraction are shown in Figure 1, using $N = 100$, $D/d = 10$, $\alpha = 0.5$, and $\varepsilon_{pn} = 0.5$. As discussed previously, the results are not sensitive to the precise values of the latter variables.[4] For the *fixed* η_t model, the bulk modulus decreases rapidly with η_n and is massively reduced at high filler loadings, trends we find physically implausible for a constant pressure equation-of-state property. In strong contrast, there is a very modest reduction based on the adjusted η_t model. For example, at $\eta_n = 0.1$ the normalized bulk modulus decreases by ~2% for the adjusted model, compared to ~34% (52%) for the constant total packing fraction model of $\eta_t = 0.55$ (0.4). New experiments that measure the bulk modulus of silica-based PNCs are required to quantitatively test our calculations.

The spinodal phase diagram for the adjusted η_t model is compared with that for constant $\eta_t = 0.4$ and 0.55 models in Figure 2. In all cases, the phase diagrams show the classic depletion (bridging) phase separation at low (high) interfacial attraction and a broad miscibility window at intermediate attraction strengths. Qualitatively, the adjusted η_t results are similar to those at $\eta_t = 0.4$ which have been reported previously,[5] although the bridging demixing region shifts to higher interfacial cohesion strengths, resulting in a significant widening of the miscibility window. More dramatic changes relative to prior results are found for the fixed $\eta_t = 0.55$ system. Specifically, unusual bridging behavior occurs in the filler packing fraction regime of $\eta_n \approx 0.03-0.21$ where enhanced miscibility is predicted with increasing nanoparticle loading. This effect may be due to the initial unrealistically

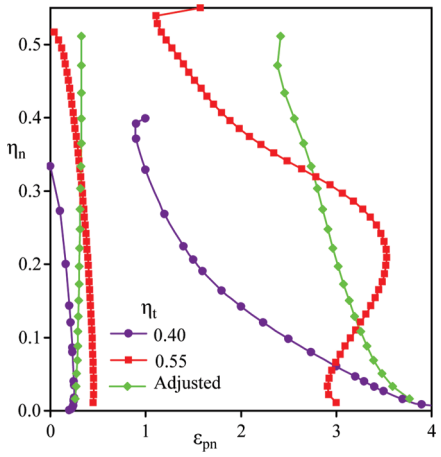

Figure 2. Filler packing fraction at the theoretical spinodal phase separation boundary as a function of interfacial attraction strength (units of thermal energy) for the three indicated mixture total packing fraction models, for $N = 100$, $D/d = 10$, and $\alpha = 0.5$.

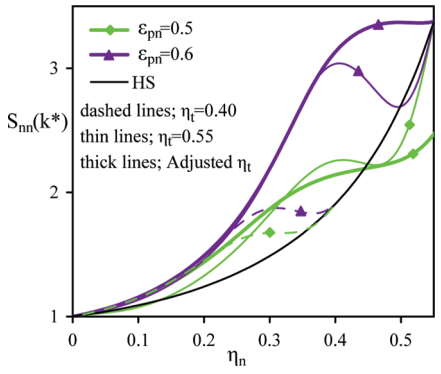

Figure 3. Intensity of the nanoparticle wide angle cage peak at $k = k^*$ as a function of filler packing fraction for the three indicated mixture total packing fraction models, for $N = 100$, $D/d = 10$, and $\alpha = 0.5$.

high and rapidly decreasing K_B of this system (or equivalently unrealistically small value of the pure melt dimensionless compressibility at atmospheric pressure) and provides further motivation for use of the adjusted η_t model.

The primary feature of the nanoparticle scattering function is the cage peak which quantifies the filler short-range order on a length scale of $2\pi/k^*$, where k^* is the wavevector at the local maximum. Calculations of the intensity of the cage peak of the filler structure factor as a function of η_n at two values of ε_{pn} in the miscibility window for the three η_t models are compared in Figure 3. The solid line shows the results for the pure hard sphere fluid (vacuum solvent). At the larger $\varepsilon_{pn} = 0.6$ for the adjusted η_t model, the bound polymer layer around each particle leads to increased cage scale order relative to pure hard spheres over the entire range of $\eta_n = 0-0.55$. At the lower $\varepsilon_{pn} = 0.5$, there is slightly less bound polymer around the nanoparticles, and the degree of filler cage ordering is decreased. At very high η_n for this system, the cage peak becomes less intense than that of pure hard spheres. Both constant total mixture packing fraction models result in nonmonotonic behavior at high filler volume fractions, a trend not seen in the experiments on PEO-based nanocomposites as will be discussed below.

Recall that our primary aim is to compare the theoretical results with experiment changing *only* the interfacial cohesion parameter ε_{pn}. The experiments were performed up to $\eta_n \approx 0.55$, so the constant $\eta_t = 0.4$ model is not applicable.

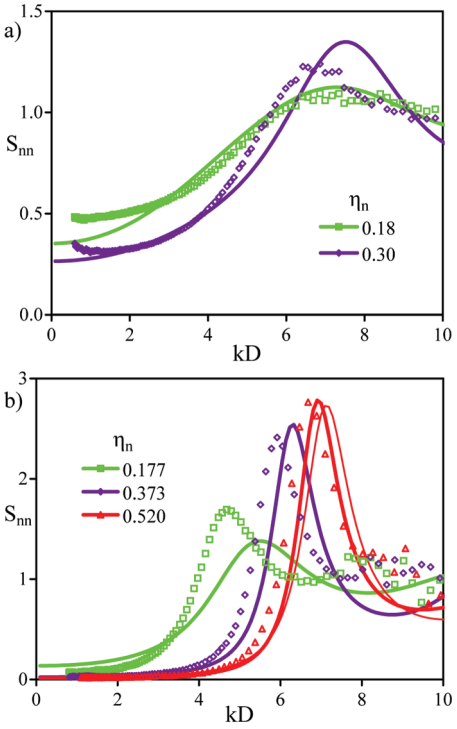

Figure 4. Collective nanoparticle structure factor as a function of dimensionless wavevector. Curves are PRISM theory results for $N = 100$, $D/d = 10$, $\alpha = 0.5$: (a) $\varepsilon_{pn} = 0.35$ and (b) $\varepsilon_{pn} = 0.55$ at various filler packing fractions. Thick lines use the adjusted η_t model; thin line for $\eta_n = 0.52$ is at $\eta_t = 0.55$. Symbols indicate experimental data for (a) silica−PTHF (MW = 1000) and (b) silica−PEO (MW = 1000).

For both constant total volume fraction models, the pure hard-sphere fluid result must be obtained as $\eta_n \rightarrow \eta_t$. However, a significant amount of polymer continues to be present in the experimental system even at $\eta_n \approx 0.55$. This is yet another reason that the adjusted packing fraction model is more appropriate to describe the experimental data.

IV. Filler Collective Scattering: Comparison of Theory and Experiment

Figure 4 presents experimental nanoparticle structure factors for (a) silica−PTHF and (b) silica−PEO (MW = 1000, $N \sim 23$) at several filler packing fractions;[6] the complementary theoretical results for the adjusted η_t model at the same packing fractions ($\eta_n/\eta_t = 0.37$ and 0.56 for PTHF and 0.37, 0.65, and 0.81 for PEO) are also shown. As more particles are added to the nanocomposite, the structure factor shows enhanced local ordering (larger $S_{nn}(k^*)$) on a smaller length scale (larger k^*). The other interesting feature is $S_{nn}(k=0)$, the filler dimensionless osmotic compressibility. Typically, the structure factor plateaus at low wavevector, though in the PTHF system at $\eta_n = 0.3$ a small upturn is seen at low k, signaling the system may be near phase separation. These long wavelength filler concentration fluctuations are enormously larger in the less interfacially cohesive PTHF system compared to the PEO−silica mixture.

The theoretical interfacial attraction strength has been adjusted to optimize agreement (by eye) of theory and experiment for $S_{nn}(k)$. We find moderate degrees of attraction: $\varepsilon_{pn} = 0.35$ for PTHF and $\varepsilon_{pn} = 0.55$ for PEO. Overall, theory and experiment qualitatively, or nearly quantitatively, agree for all features over all length scales. The results at fixed $\eta_t = 0.55$ are qualitatively similar, especially at low packing fractions; a representative example at the highest packing fraction (thin line in Figure 4b) shows the small change compared to the adjusted η_t model. However, as mentioned above, the shape of the $S_{nn}(k^*)$ vs η_n

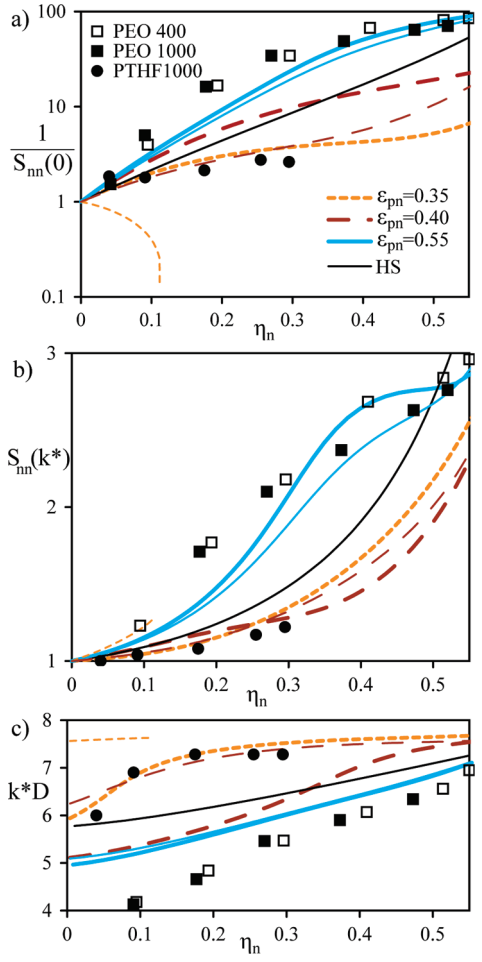

Figure 5. (a) Inverse of the nanoparticle dimensionless osmotic compressibility, (b) height of the cage peak of the nanoparticle structure factor, and (c) the corresponding peak wavevector, as a function of filler packing fraction. Colored (thick ($N = 100$), thin ($N = 10$)) PRISM curves are for $D/d = 10$, $\alpha = 0.5$ based on the adjusted η_t model; black curve is for a pure hard-sphere fluid (polymer replaced by vacuum). Experimental data are for silica−PEO (squares) and silica−PTHF (circles) of MW = 400 (open squares) and 1000 (solid symbols).

curve does show a qualitative difference between these models. Note that the $\varepsilon_{pn} = 0.55$ mixture is in the miscibility window of Figure 2, though relatively close to the depletion phase separation boundary (depletion first occurs just below $\varepsilon_{pn} = 0.33$). This theoretical result is consistent with the experimental observation[6] of full miscibility to extremely high nanoparticle volume fractions for the silica−PEO mixture. In contrast, the $\varepsilon_{pn} = 0.35$ system lies very close to depletion phase separation, and the experimental silica−PTHF system is observed to form a nonequilibrium solid (gel) at $\eta_n \approx 0.3$.

Figure 5 compares theory and experiment for the three characteristic features of the collective filler structure factor of the PEO- and PTHF-based nanocomposites: inverse dimensionless osmotic compressibility, $S_{nn}^{-1}(k = 0)$, and the intensity, $S_{nn}(k^*)$, and location, k^*, of the cage peak. The analogous reference hard sphere fluid results are also shown. Consider first the two PEO systems. The theoretical results based on the adjusted total packing fraction model qualitatively or quantitatively agree with all the experimental trends: (i) little variation with degree of polymerization (N) for the more miscible system, emphasizing the locality of the physics under equilibrium conditions, (ii) reduced long wavelength concentration fluctuations, and (iii) greater cage scale order on a larger length scale (smaller k^*) relative to the pure hard-sphere fluid analogue. The latter two trends reflect polymer-mediated nanoparticle ordering due to thermodynamically stable bound polymer layers which result in the fillers appearing effectively larger than their bare diameter.[4,5] Quantitatively, at intermediate (low) packing fractions $S_{nn}(0)$ ($S_{nn}(k^*)$) is modestly overpredicted (underpredicted), and the cage size is a bit too small although the nearly linear variation of k^* with η_n is well captured.

To illustrate the remarkable sensitivity of the nanoparticle collective structure factor to interfacial cohesion strength predicted by the theory, and make contact with the new measurements on the silica−PTHF nanocomposite, calculations for two modestly smaller values of ε_{pn} are also shown in Figure 5. One expects the latter systems have a weaker adsorbed polymer layer, resulting in less cage scale order (lower $S_{nn}(k^*)$) of smaller characteristic length scale (higher k^*), and a greater tendency for depletion aggregation (higher concentration fluctuations, $S_{nn}(k = 0)$). All these expectations are borne out by the calculations and experiments. As ε_{pn} decreases, the macroscopic nanoparticle concentration fluctuations do intensify and are much larger than their pure hard-sphere analogues, especially at high η_n. The cage peak weakens indicating reduced local order that is significantly less than the equivalent hard-sphere fluid. For $\varepsilon_{pn} = 0.35$ and $N = 100$, the magnitudes of $S_{nn}(0)$, $S_{nn}(k^*)$, and k^*, and their dependence on η_n, are remarkably similar to the silica−PTHF data, thereby providing a consistent description of nanoparticle collective concentration fluctuations over all scales. Note that the average length scale of order decreases, and k^* is no longer linear with η_n.

Recall that adjusting ε_{pn} in the theory corresponds to changing the monomer-level *effective* attraction between the nanoparticle and polymer. The high sensitivity of the filler collective scattering patterns to the magnitude of the interfacial attraction allows the theory to be used as a tool to deduce ε_{pn} which otherwise is not directly measurable experimentally. Since the polymer−polymer and particle−particle interactions are hard-core, ε_{pn} is proportional to the net reduction in energy upon transferring a monomer from a pure polymer environment to being in contact with the silica surface. Although the chemistry of silica, PEO, and PTHF is complex, a simple model for ε_{pn} is to assume most of the polymer−particle attraction arises from hydrogen bonding between the hydroxyl group on the silica surface and the oxygen in the polymer. Specifically, PEO $(-C_2H_4O-)_N$ and PTHF $(-C_4H_8O-)_N$ are chemically similar except for the ratio of CH_2 groups to oxygen; PEO is 36 wt % oxygen, while PTHF is 22 wt % oxygen. Hence, we crudely estimate the PTHF attraction is ~60% that of PEO, yielding $\varepsilon_{pn} = 0.6 \times 0.55 \sim 0.35$ for PTHF. This a priori estimate is remarkably consistent with the adsorption energy required for PRISM theory to reproduce well all the features of the PTHF nanocomposite scattering patterns in Figure 5.

At lower $N = 10$, the theory compares best to the PTHF data when $\varepsilon_{pn} \sim 0.4$ rather than 0.35. This modest difference is likely primarily a reflection of the limitation of the ideal freely jointed chain model used in PRISM theory. As the theoretical model systems which agree well with the PHTF scattering data are very close to the depletion phase boundary (at $\varepsilon_{pn} = 0.35$ the $N = 10$ mixture is not miscible beyond $\eta_n = 0.11$), it is not unreasonable that the previously minor effect of N for the PEO mixture is exaggerated for its PTHF analogue and coupled to the value of ε_{pn}. Within the theory, a primary effect of lowering N is to increase the bulk modulus: the $N = 10$ system appears slightly denser in the sense that interchain packing is better due to less intrachain overlaps[3,11] and therefore experiences stronger depletion attraction than at $N = 100$. In real constant pressure systems, the bulk modulus should be approximately N-independent, so lowering the $N = 10$ polymer density would likely make the $N = 10$ nanocomposite results even closer to those at $N = 100$. We do

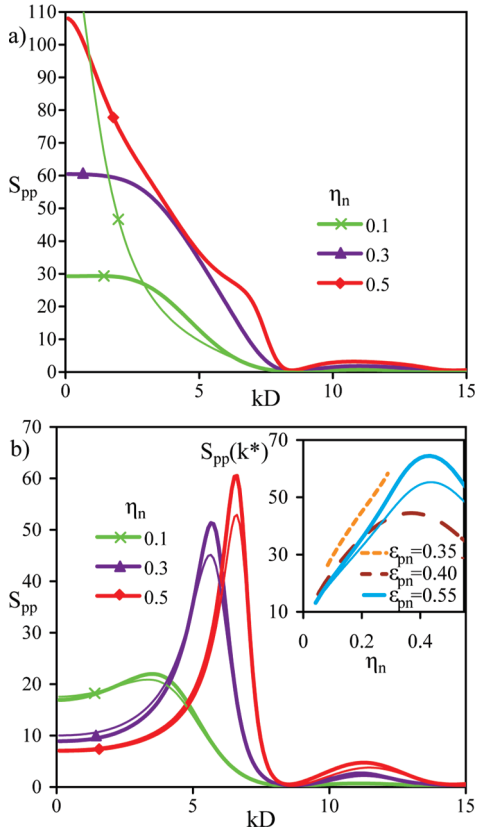

Figure 6. Theoretical polymer collective structure factor for $N = 100$ (thick lines) and $N = 10$ (thin lines), $D/d = 10$, $\alpha = 0.5$, adjusted η_t model: (a) $\varepsilon_{pn} = 0.35$ and (b) $\varepsilon_{pn} = 0.55$. Inset shows the intensity of the microphase-like peak (if present) as a function of total packing fraction for three values of ε_{pn}.

not further explore this small second-order effect because it is not important for the comparisons we wish to make. The $N = 10$, $\varepsilon_{pn} = 0.35$ results show the mixture is approaching phase separation since $S_{nn}(0)$ increases sharply with η_n, and the cage peak is more intense and occurs at a higher wavevector than in the miscible case. All these trends reflect local nanoparticle aggregation as a precursor to depletion phase separation.

V. Polymer Collective Small-Angle Scattering

We now employ the theory using the *same* model parameters determined in section IV to make predictions for the *polymer* collective concentration fluctuations as encoded in $S_{pp}(k)$. This quantity is amenable to measurement using small-angle neutron scattering and deuterium labeling. Figure 6a shows the polymer collective structure factor for the PTHF system ($\varepsilon_{pn} = 0.35$), while Figure 6b shows the corresponding results for PEO ($\varepsilon_{pn} = 0.55$). For the PEO system the fillers are surrounded by a strongly held bound polymer layer. As a consequence, an intense low wavevector, or "microphase separation like", peak emerges on a length scale controlled (to first order) by nanoparticle size. Its physical origin is an "imprinting" of filler order on the structurally perturbed adsorbed polymer layers.[4,5,20] The microphase peak location, $k^* \sim 2\pi/D$, shifts to higher wavevector, but its amplitude varies nonmonotonically, with increasing nanoparticle concentration. These trends arise from a compression of the bound layer around the filler and increasing interfiller interference as nanoparticle loading increases. The long wavelength concentration fluctuations for the silica−PEO system (Figure 6b) first decrease with increasing nanoparticle volume fraction and then become nearly constant. There is little N dependence of $S_{pp}(k)$ for this miscible system, though lowering N slightly decreases the microphase peak and increases $S_{pp}(0)$.

At $\varepsilon_{pn} = 0.35$ relevant to the PTHF mixture, there is less adsorbed polymer, and therefore the peak in Figure 6a sometimes disappears or is only a shoulder. A feature at nonzero k^* may still exist with significant amplitude but is effectively "buried" under the large-amplitude $k = 0$ peak associated with the osmotic compressibility contribution. The $N = 10$, $\eta_n = 0.1$ system is similar to its $N = 100$ analogue at large wavevectors but has even less bound polymer since it is closer to the depletion spinodal. Thus, no discernible shoulder in $S_{pp}(k)$ is seen as it sharply increases toward the $k = 0$ limit; this mixture is nearing spinodal phase separation and at higher η_n is immiscible.

The inset of Figure 6b shows the detailed variation of the microphase order parameter, $S_{pp}(k^*)$, with filler volume fraction. For the $\varepsilon_{pn} = 0.35$ system that mimics the silica−PTHF nanocomposite, when a local maximum is present at $N = 100$, its intensity grows approximately linearly with η_n at intermediate filler loadings, but this maximum disappears at low and high η_t (and at all η_t for $N = 10$). Thus, a sharp filler scale peak in the polymer scattering may serve as an experimentally measurable indicator of the existence of a bound polymer layer with properties (e.g., local density) distinct from the bulk polymer melt far from filler surfaces. At $\varepsilon_{pn} = 0.55$, the microphase order parameter first increases roughly linearly with η_n reflecting the growing amount of perturbed adsorbed polymer. However, $S_{pp}(k^*)$ then goes through a maximum and decreases at very high filler packing fractions. The latter trend occurs at both $N = 10$ and 100, although the value of the peak is somewhat smaller at lower N. We interpret this decrease in $S_{pp}(k^*)$ as arising from the overlap or sharing of bound layers on different nanoparticles and the fact that most polymers are associated with filler and their total amount decreases with η_n.

VI. Polymer-Mediated Filler Potential of Mean Force and Kinetic Arrest

To gain insight concerning the real space nanoparticle organization, Figure 7 presents calculations of the nanoparticle potential of mean force, $W_{nn}(r) = -\ln(g_{nn}(r))$, for the *same* systems as in Figure 6. With increasing nanoparticle volume fraction, the PMF has a deeper contact attraction and lower repulsive barrier, which reflects the many body interference of adsorbed polymer layers around different fillers. Lowering ε_{pn} from 0.55 to 0.35 enhances the contact depletion attraction and reduces the monomer scale oscillations in the PMF, presumably due to less bound layer interference between particles. Decreasing N from 100 to 10 exaggerates the monomer scale oscillations in W_{nn} (not shown) for both ε_{pn} values, since the shorter polymer fluid appears more locally dense (higher bulk modulus) when compared at the same theoretical packing fraction. This leads to qualitatively similar behavior but larger minima in the PMF at lower N.

The inset of Figure 7b plots the *global* minimum of W_{nn} as a function of η_n for both $N = 10$ and 100. At $N = 100$, low η_n and $\varepsilon_{pn} = 0.55$, the global minimum of the PMF corresponds to filler "bridging" at an interparticle surface-to-surface separation of roughly two monomer diameters. As η_n increases, the bridging minimum weakens, and the contact aggregation minimum deepens, ultimately becoming the global minimum beyond $\eta_n \approx 0.23$. The global minimum when $\varepsilon_{pn} = 0.35$ and 0.4 is always at particle contact since there is less interfacial attraction to overcome entropic depletion and the driving force for bridging is weaker.

Although PRISM is an equilibrium theory, recent progress in the area of sticky colloid suspensions[21] suggests that when the minimum in $W_{nn}(r)$ becomes sufficiently deep (~4−5 kT) interparticle collisions can become irreversible on the experimental

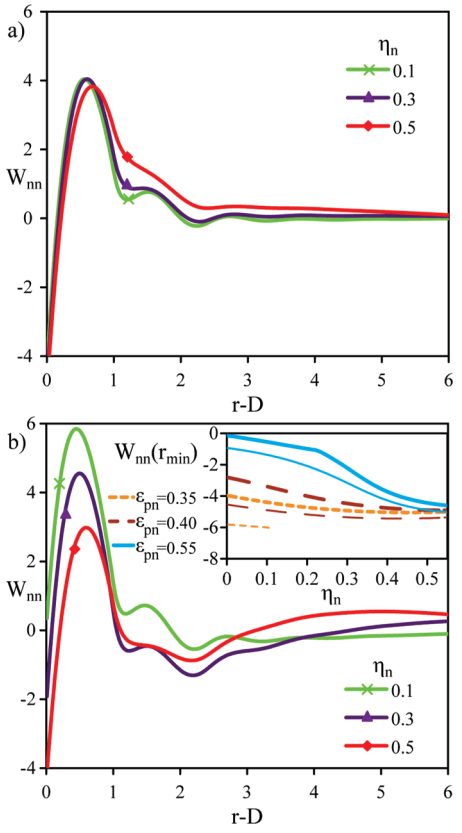

Figure 7. Nanoparticle potential of mean force (units of kT) as a function of surface-to-surface separation for $N = 100$, $D/d = 10$, $\alpha = 0.5$, adjusted η_t model, and (a) $\varepsilon_{pn} = 0.35$ and (b) $\varepsilon_{pn}=0.55$. Inset of (b) shows the value of the global minimum of W_{nn} as a function of nanoparticle packing fraction for various ε_{pn} at $N=100$ (thick lines) and $N = 10$ (thin lines).

time scale, resulting in a kinetically arrested "gel". On the basis of this scenario, the results in Figure 7 suggest that the lower ε_{pn} systems (silica−PTHF) may form a gel at relatively low η_n, in contrast to the $\varepsilon_{pn} = 0.55$ system (silica−PEO) which should remain stable up to high η_n. This theoretical deduction is qualitatively consistent with rheological measurements[6,22] which find a gel-like transition in silica−PTHF at $\eta_n \sim 0.265$, while PEO samples are fluid. Moreover, the nonequilibrium kinetic arrest appears to be correlated with the greatly enhanced long wavelength nanoparticle concentration fluctuations (large $S_{nn}(k=0)$) as seen in Figure 5, a trend which is properly captured by the theory. Such a connection between gelation due to contact particle aggregation and incipient phase separation has been emphasized in recent studies of suspensions of attractive spherical particles.[23]

VII. Summary

To the best of our knowledge, we have presented the first systematic combined theory−experiment quantitative analysis of adsorbing and bridging polymer-mediated structural organization of nanoparticles in miscible polymer nanocomposites. The microscopic statistical mechanical theory can qualitatively, and in some cases nearly quantitatively, account for the observed structural effects over a wide range of length scales, filler volume fractions, and variable interfacial cohesion. Prior PRISM theory work explored only a mixture model at constant total packing fraction of 0.4[4,5]or 0.5.[14,15] However, the scattering of silica particles in PEO was measured up to nanoparticle packing fractions of 55%, thereby motivating the formulation of a different model for the PNC total packing fraction. Specifically, in order to mimic the expected constant pressure equation-of-state effects, we propose to increase the total mixture packing fraction as nanoparticles are added to the polymer melt in such a manner that the polymer packing fraction in the space available to monomers is constant. This "adjusted packing fraction" model results in a significantly reduced (and physically sensible) variation of the nanocomposite bulk modulus with filler loading and improved agreement with the experimental structure factors. The theoretical trend in the particle osmotic compressibility as a function of filler packing fraction is qualitatively similar to experiment, as is the height and location of the particle cage peak in the structure factor. The predicted changes in these structural quantities with decreasing interfacial attraction match well the dramatic effects observed in experiment when the more weakly adsorbing PTHF is used. Both theory and experiments at low molecular weights show little dependence of nanoparticle concentration fluctuations on chain length.

The spinodal phase boundary for the adjusted packing fraction model was obtained and compared to that at constant packing fractions of 0.55 and 0.4. Significant quantitative differences are found, especially on the bridging side of the phase diagram. However, the most striking aspect that a miscibility window exists remains true.

A prior comparison of PRISM theory to small-angle neutron scattering experiments on a silica−polystyrene nanocomposite up to volume fractions of 0.3 suggested the existence of a "microphase-like" peak on the filler length scale in the *collective polymer* structure factor.[20] The theoretical phase diagram, particle structure factors, and filler potential of mean force have also been reported previously but only under constant total packing fraction conditions.[4,5] Besides performing the first theory/experiment comparison of collective nanoparticle scattering, and introducing the more realistic adjusted total packing fraction model, our present work specifically places the PEO−silica and PTHF−silica systems on the generic theoretical phase diagram. In contrast to the PEO−silica mixture, we predict the PTHF−silica nanocomposite is very near depletion phase separation and will not display the polymer microphase peak observed for miscible systems. Hence, this peak may be used as an experimental indicator of the presence of a bound polymer layer and the attendant steric stabilization. The theoretical potential of mean force for the PEO and PTHF nanocomposites were also computed and indicate the PTHF system has a very strong depletion minimum which is consistent with the experimental observation of nonequilibrium gelation at high enough filler loadings.

Finally, the ability of PRISM theory to predict rather well concentration fluctuations over all length scales provides a foundation for the future development of microscopic statistical mechanical theories of slow dynamics, kinetic arrest, and mechanical properties of molten polymer nanocomposites.

Acknowledgment. This work was supported by the Nanoscale Science and Engineering Initiative of the National Science Foundation under NSF Award DMR-0642573.

References and Notes

(1) Winey, K. I.; Vaia, R. A. *MRS Bull.* **2007**, *32*, 314–319. Schadler, L. S.; Kumar, S. K.; Benicewicz, B. C.; Lewis, S. L.; Harton, S. E. *MRS Bull.* **2007**, *32*, 335–340.
(2) Mackay, M. E.; Tuteja, A.; Duxbury, P. M.; Hawker, C. J.; Van Horn, B.; Guan, Z. B.; Chen, G. H.; Krishnan, R. S. *Science* **2006**, *311*, 1740–1743.
(3) Schweizer, K. S.; Curro, J. G. *Adv. Chem. Phys.* **1997**, *98*, 1.
(4) Hooper, J. B.; Schweizer, K. S. *Macromolecules* **2005**, *38*, 8858−8869; **2006**, *39*, 5133−5142; **2007**, *40*, 6998−7008.
(5) Hall, L. M.; Schweizer, K. S. *J. Chem. Phys.* **2008**, *128*, 234901.
(6) Anderson, B. J.; Zukoski, C. F. *Macromolecules* **2008**, *41*, 9326–9334.

(7) Anderson, B. J.; Zukoski, C. F. *Macromolecules* **2007**, *40*, 5133–5140.
(8) Smith, G. D.; Yoon, D. Y.; Jaffe, R. L.; Colby, R. H.; Krishnamoorti, R.; Fetters, L. J. *Macromolecules* **1996**, *29*, 3462–3469.
(9) Wick, C. D.; Theodorou, D. N. *Macromolecules* **2004**, *37*, 7026–7033.
(10) Rubinstein, M.; Colby, R. H. *Polymer Physics*; Oxford University Press: New York, 2003.
(11) Curro, J. G.; Schweizer, K. S.; Grest, G. S.; Kremer, K. *J. Chem. Phys*. **1989**, *91*, 1357–1364.
(12) Chandler, D.; Andersen, H. C. *J. Chem. Phys*. **1972**, *57*, 1930–1937.Chandler, D. *Studies in Statistical Mechanics*; Lebowitz, J. L., Montroll, E. W., Eds.; North-Holland: Amsterdam, 1982; pp 275−340.
(13) Hooper, J. B.; Schweizer, K. S.; Desai, T. G.; Koshy, R.; Keblinski, P. *J. Chem. Phys*. **2004**, *121*, 6986–6997.
(14) Zhao, L.; Li, Y.-G.; Zhong, C.; Mi, J. *J. Chem. Phys*. **2006**, *124*, 144913.
(15) Zhao, L.; Li, Y.-G.; Zhong, C. *J. Chem. Phys*. **2007**, *126*, 014906.
(16) Biben, T.; Hansen, J.-P. *Phys. Rev. Lett*. **1991**, *66*, 2215–2218.
(17) Lekkerkerker, H. N. W.; Stroobants, A. *Physica A* **1993**, *195*, 387–397.
(18) Roth, R.; Evans, R.; Louis, A. A. *Phys. Rev. E* **2001**, *64*, 051202.
(19) Hansen-Goos, H.; Roth, R. *J. Chem. Phys*. **2006**, *124*, 154506.
(20) Sen, S.; Xie, Y.; Kumar, S. K.; Yang, H.; Bansal, A.; Ho, D. L.; Hall, L.; Hooper, J. B.; Schweizer, K. S. *Phys. Rev. Lett*. **2007**, *98*, 128302.
(21) Dawson, K. A. *Curr. Opin. Colloid Interface Sci*. **2002**, *7*, 218–227. Bergenholtz, J.; Poon, W. C. K.; Fuchs, M. *Langmuir* **2003**, *19*, 4493–4503. Chen, Y. L.; Schweizer, K. S. *J. Chem. Phys*. **2004**, *120*, 7212–7222.
(22) Anderson, B. J.; Zukoski, C. F., manuscript in preparation.
(23) Lu, P. J.; Zaccarelli, E.; Cuilla, F.; Schofield, A. B.; Sciortino, F.; Weitz, D. A. *Nature* **2008**, *453*, 499−504, and references cited therein.